Journal of the Brazilian Society of Mechanical Sciences and Engineering (2019) 41:313
https://doi.org/10.1007/s40430-019-1802-z

TECHNICAL PAPER

Evaluation of double-layer weld deposition technique on ASTM A182 F22 steel without post-weld heat treatment

Douglas Neves Garcia[1] · Valtair Antônio Ferraresi[2] · Carlos Alberto Mendes da Mota[3]

Received: 5 February 2019 / Accepted: 6 June 2019 / Published online: 10 July 2019

Abstract
The present work evaluates the mechanical and metallurgical behavior of ASTM A182 F22 steel heat-affected zone (HAZ) through the double-layer weld deposition technique, with different welding energies between the first and second layers. This methodology leads to the reduction of hardness levels in the HAZ and can exempt the need for post-weld heat treatment on low-alloy steel after buttering welding. The welding was performed by the automated GMAW process in flat position. As the filler metal, the AWS ER309L, ER 80S-G and ER NiCrMo-3 (Inconel 625) alloys were applied on ASTM A182 F22 steel. The analysis of the refining and/or tempering in coarse-grained HAZ (CGHAZ) of the first layer was performed by metallographic tests and microhardness measurements. The tempering of the first-layer CGHAZ is dependent on the correct overlap of the weld layers, weld bead geometry and the highest imposed heat of the second layer. The results revealed that the Higuchi technique is effective for obtaining welding parameters for the second-layer deposition that promotes thermal treating of the hard region of the first-layer HAZ. However, this technique was not able to reduce the hardness values at the 250 HV level required by NACE 0175 for the test conditions in this work.

Keywords ASTM A182 F22 Steel · Higuchi test · Double-layer

1 Introduction

A Cr–Mo high-strength low-alloy (HSLA) steel is a creep-resistant metal commonly used as forged and was initially developed for use in the petroleum industry and power generation plants [1, 2], although today it is already used in the manufacture components of submarine oil wells. The Cr and Mo addition has a purpose to form a tenacious alloy with good creep and corrosion resistance when compared to carbon steels [3, 4]. It also presents good weldability although re-heating and cold cracking may occur in the HAZ [1–6].

The ASTM A182 F22 steel is used in the offshore industry in normalized condition, when the heat treatment is conducted after forging to enable a uniform and refined microstructure. In the normalizing heat treatment, this steel is heated just above the temperature of A3 line, in order to avoid grain growth. This results in a fine austenite grains nucleation, as well as the dissolution of carbides formed during cooling from the forging. A 2.25Cr–Mo steel presents, after normalizing heat treatment, a mixed microstructure of ferrite and bainite besides the presence of carbides [1–6].

F22 steel has an equivalent carbon (EC) of 0.8, which, according to the literature [7], is highly susceptible to cracking and requires care in the choice of welding parameters and filler metal. In addition, it needs preheating, control of the temperature between passes and post-weld heat treatment (PWHT) [7–9].

The welding process changes the microstructure in the HAZ of HSLA steel. This microstructural change, mainly in the coarse-grained region, can lead to a high-hardness phase formation (bainite and/or martensite), increasing this property and reducing the ductility. The low-tenacity microstructure formation depends on the thermal cycle imposed and the cooling rate, where the cooling rates above 100 K/s

Technical Editor: Lincoln Cardoso Brandão.

✉ Douglas Neves Garcia
dgarcia@ufpa.br

[1] FEM-Faculty of Mechanical Engineering, Federal University of Pará (UFPA), Tucuruí, PA 68464-000, Brazil

[2] Laprosolda-Center for Research and Development of Welding Processes, Federal University of Uberlandia (UFU), Uberlândia, MG 38408-100, Brazil

[3] Getsolda-Group of Studies in Welding Technology, Federal University of Pará (UFPA), Belém, PA 66075-110, Brazil

will form the martensite microstructure in the steel. With lower cooling rates, the steel is transformed into bainite. Besides, with cooling rates below 1 K/s, the ferrite presence with different proportions of bainite is observed [2].

In order to relieve the mechanical properties and toughness variations in the welded joints HAZ formed in F22 steel, PWHT is commonly employed. However, when the F22 is welded with a different chemical composition filler metal (dissimilar welding), the HSRT in dissimilar joint leads to a carbon migration from HAZ to the dissimilar interface, resulting in carbon enrichment in this region, which may lead to martensite formation, as well as carbides, contributing to a toughness loss in a rich hydrogen environment [10–12].

Based on this context, there is a need to find an alternative to reduce HAZ hardness and reduce or eliminate carbon migration to dissimilar interface. The two-layer technique presents a good option, as shown in Fig. 1, as the heat generated by the second-layer deposition can promote the refining and/or tempering of the first-layer coarse-grained heat-affected zone (CGHAZ), reducing the hardness and increasing the strength [13–18].

The successful use of double-layer technique is related to a correct relationship between the welding energies in the first and second layers, as well as the initial and interpass temperatures' control and a suitable overlap the weld beads. The Higuchi test [19] proved to be a satisfactory tool to choose the weld heat input ratios (Fig. 1). The test is to meet the two conditions of Eqs. 1 and 2:

$$\begin{aligned} &1\text{st condition) } SZD2 > HZD1 : \\ &\Delta 1 = SZD2 - HZD1; (+)\text{Attended} \\ &(-)\text{Not Attended} \end{aligned} \tag{1}$$

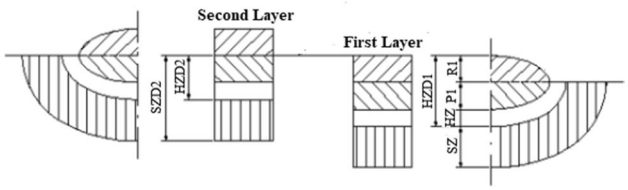

Fig. 1 Representation of Higuchi test criteria [19]

SZD2 is the depth of second-layer soft zone, and HZD1 is the depth of first-layer hard zone.

$$\begin{aligned} &2\text{nd condition) } HZD2 < R1 + P1 : \\ &\Delta 2 = (R1 + P1) - HZD2; \\ &(+)\text{Attended}(-)\text{Not Attended} \end{aligned} \tag{2}$$

HZD2 is the depth of second-layer hard zone, R1 is the reinforcement of the first layer and P1 is the penetration of the first layer.

The fulfillment of the first condition means that the heat imposed by the second-layer deposition quenches and/or refines the first-layer CGHAZ, while the compliance with the second condition ensures that the first-layer hard zone will not be austenitized and re-tempered.

The present work aims to evaluate the efficiency of double-layer welding technique on F22 steel, without PWHT, in terms of the HAZ microstructural and hardness changes, besides evaluating the carbon migration in the weld interface, and compare the results with PWHT.

2 Materials and methods

The GMAW (gas metal arc welding) process was selected for this research, due to its high productivity and for being widely used in the production of parts for offshore industry. The tests were carried out on ASTM A182 F22 steel plates, and the filler metals were ER NiCrMo-3, ER 309L-Si and ER 80S-G, with 1.2 mm in diameter. The chemical compositions of the base metal and filler metals are shown in Table 1. The ER 80S-G filler metals were used to perform a metallurgical study on this material bonding zone with the F22 steel and to compare with the dissimilar interface microstructure formed by the F22 steel and the ER NiCrMo-3 (Inconel 625) wire, normally used in the standard procedure in the oil extraction and refining industry. Another point of interest on the employment of the ER 80S-G and 309L-Si wires is the economical factor, since the substitution of Ni alloys by less noble materials would decrease the production cost of the welded joint.

This work methodology was carried out in two stages. First, single passes were deposited on F22 steel plates by Higuchi test procedure. After, double-layer welds were performed on F22 steel plates with weld conditions approved in

Table 1 Chemical composition of the base (F22) and filler metals (NiCrMo-3, 309L-Si and 80S-G). Manufacturer data

	C	Mn	Cr	Ni	Mo	Si
F22 steel	0.09	0.38	2.12	0.16	0.97	0.16
NiCrMo3 wire	0.1	0.5	21.5	58.0	9.0	0.5
309L-Si wire	0.03	1.8	23.5	13.5	0.4	0.9
80S-G wire	0.08	1.1	0.4	0.5	–	0.6

the Higuchi method, to evaluate the tempering and/or refinement effect in first-layer CGHAZ.

2.1 Higuchi test

In this step, welding was carried out in single passes on F22 steel plates with 100 × 30 × 10 mm, in flat position with the automated GMAW process. The dimensions of the base metal were defined after preliminary tests to determine the extension of the HAZ for different welding energies used. The preheating temperature was maintained in 250–300 °C range, in accordance with the values (150–315 °C) recommended by ASTM A182 standard [9]. Preheating was performed using an electric resistance and a blanket. An infrared digital thermometer was used to regulate the temperature.

Figure 2 shows the base metal microstructure with bainitic/ferritic structure containing thin carbides dispersed throughout in the matrix. This observation is consistent with the literature [1–6]. The X-ray diffraction pattern (Fig. 3) obtained from the base metal reveals bainite and ferrite characteristic peaks.

The welding parameters used in single-pass deposition with different filler metals were selected after a series of bead-on-plate weld tests in order to find operational parameters capable of producing weld beads with good geometric regularity and absence of superficial defects.

Therefore, after these exploratory tests, an experiment table was set up, as shown in Table 2, including the welding parameters that generated satisfactory quality weld beads. The energy variations on the welding processes were a consequence of the different wire feed (current) and welding speeds employed. It is worth mentioning that the differences observed on the electrical signals with the change of the filler metal are also a function of the different gases used,

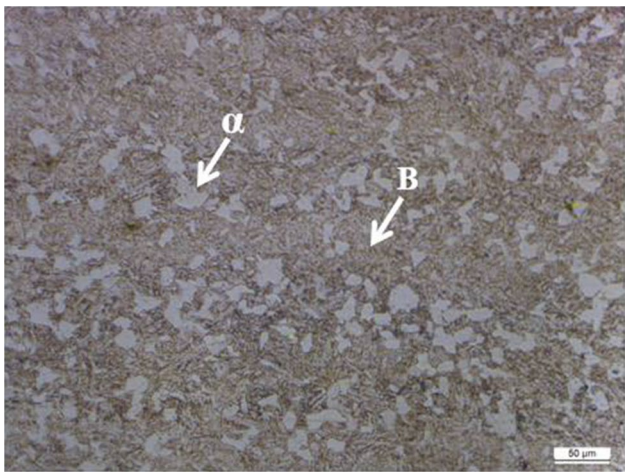

Fig. 2 Microstructure of F22 steel, as received

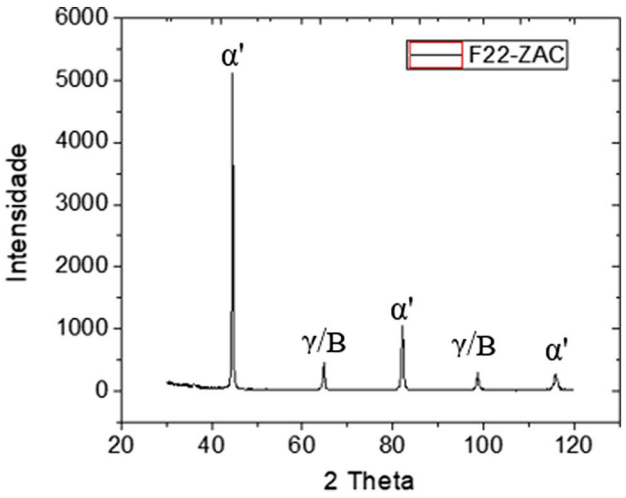

Fig. 3 Diffractogram of F22 steel obtained through X-Ray diffraction test

such as pure argon for Inconel 625 wire, $CO_2 + 25\%$ Ar for ER 80S-G wire and Ar-2% O_2 for the 309L-Si wire, and, consequently, different metal transfer modes. Heat input was calculated according to Eq. 3.

$$H = \left(\frac{V \cdot I}{v}\right)\eta \tag{3}$$

where H is the heat input (J/mm); V is the tension (V); I is the electrical current (A); v is the welding speed (mm/s); η is the thermal efficiency of the welding process. (0.8 is the usual value for GMAW.)

After welding, the weld beads were cross-sectioned and three transversal samples were taken from different regions (start, middle and end of the weld bead), for metallographic preparation to evaluate the microhardness profiles and define the hard and soft zones (Fig. 4). The base metal average hardness used in Higuchi test was 220 HV. The values of 310 and 220 HV were used to delimit the extension of hard (HZ) and soft (SZ) zones. In this way, the ZD was characterized by hardness above 310 HV, while the SZ presented values between 220 and 310 HV.

The load used in the microhardness test was 100 g, and the distance between the impressions was 0.1 mm. The reinforcement measurement and weld bead penetration were performed by using ImageJ software.

2.2 Double layer

The decision diagram was used to select the correct energy relations for the first- and second-layer welds indicated by Higuchi's test. This tool facilitates the graphical visualization of the countless possibilities for the welding parameter combinations used in the double-layer technique, allowing

Table 2 Single-pass welding parameters. First step, Higuchi test

Condition	Electrode wire	Wire speed (m/min)	Welding speed (cm/min)	Current (A)	Tension (V)	Welding heat input (J/mm)
N1	Inconel 625	5.0	30	164	27.7	726.8
N2	Inconel 625	5.0	40	151	24.8	449.2
N3	Inconel 625	6.0	30	177	26.6	753.3
N4	Inconel 625	6.0	40	176	26.3	555.2
N5	Inconel 625	4.3	30	136	26	565.8
N6	Inconel 625	4.3	40	134	27.7	445.2
I1	309L-Si	6.0	30	210	27	907.2
I2	309L-Si	6.0	40	210	27	680.1
I3	309L-Si	6.0	50	210	27	544.5
I4	309L-Si	8.0	30	280	31	1388.8
I5	309L-Si	8.0	40	280	31	1041.1
I6	309L-Si	8.0	50	280	31	833.6
C1	80S-G	3.3	20	150	23	828.8
C2	80S-G	3.3	30	150	23	552.0
C3	80S-G	5.0	20	200	24	1153.1
C4	80S-G	5.0	30	200	24	768.0
C5	80S-G	6.7	20	250	24	1441.4
C6	80S-G	6.7	30	250	24	960.0

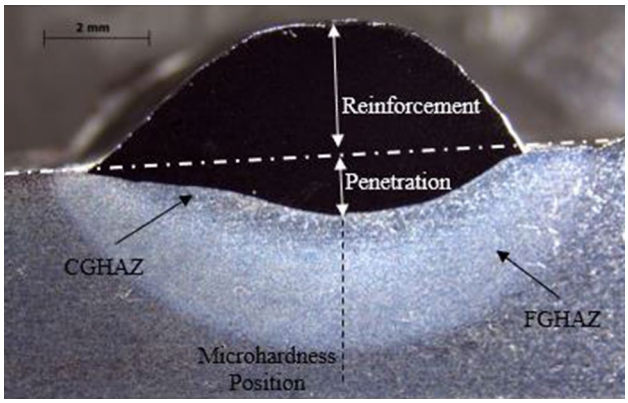

Fig. 4 Macrography of a transversal cross section of a single-pass weld bead. Geometry and microhardness profile measurement location

the correct selection of parameters that meet the conditions of Eqs. (1) and (2).

Based on the decision diagram, some welding conditions were selected in order to analyze the thermal cycling overlap efficiency in terms of hardness reduction in the first-layer CGHAZ. Some criterion for double-layer deposition was adopted on this step. First, that the deposition with the 309L-Si wire would only be possible over the Inconel 625 wire, since different authors [10, 20, 21] already reported that the carbon migration is more intense in the dissimilar interface formed with a stainless steel when compared to a dissimilar interface formed with Ni alloys. The second criterion is that no dissimilar interface should be created with the mixture of filler metals, when using ER 80S-G for double-layer deposits, in order to reduce the effects of carbon migration in the dissimilar interfaces.

Table 3 Welding parameters for double-layer deposition

Relationship energy	Condition	Layer	Welding energy (J/mm)
C1/C6	C1	First	828.8
	C6	Second	960.0
N5/I2	N5	First	565.8
	I2	Second	680.1

The welding parameters of double-layer deposition selected to validate the technique are shown in Table 3. The deposition of the first-layer lateral passes can act in a partial tempering of the HAZ, as well as in the refinement. An overlapping between 50 and 70% may be beneficial to HAZ, improving microstructure and hardness [18, 22, 23].

The Higuchi weld validation technique was made on ASTM F22 steel plates with $100 \times 50 \times 10$ mm. Double-layer welds were made with 50% overlap between passes; preheating and interpass temperatures were kept between 250 and 300 °C.

Double-layer weld samples, as given in Table 3, were also submitted to PWHT at 675 °C for 2 h, in the conditions recommended by ASTM A182 standard [9]. In this

way, it was possible to compare the effects of overlapping thermal cycles of the double-layer weld technique with the PWHT, over the tempering of the structure of the first-layer CGHAZ, along with the hardness reduction in this region.

The samples were prepared and evaluated through metallographic tests, optical microscope, scanning electron microscope and microhardness test, according to ASTM E 384 standard.

3 Results and discussion

3.1 Tests of Higuchi

From the welded joint cross-sectional microhardness profile, obtained according to the methodology presented in Fig. 4 and a Higuchi test isolated pass (Table 2), the HAZ extension can be dimensioned.

Figures 5, 6 and 7 present the microhardness profiles of the samples' cross sections welded with Inconel 625,

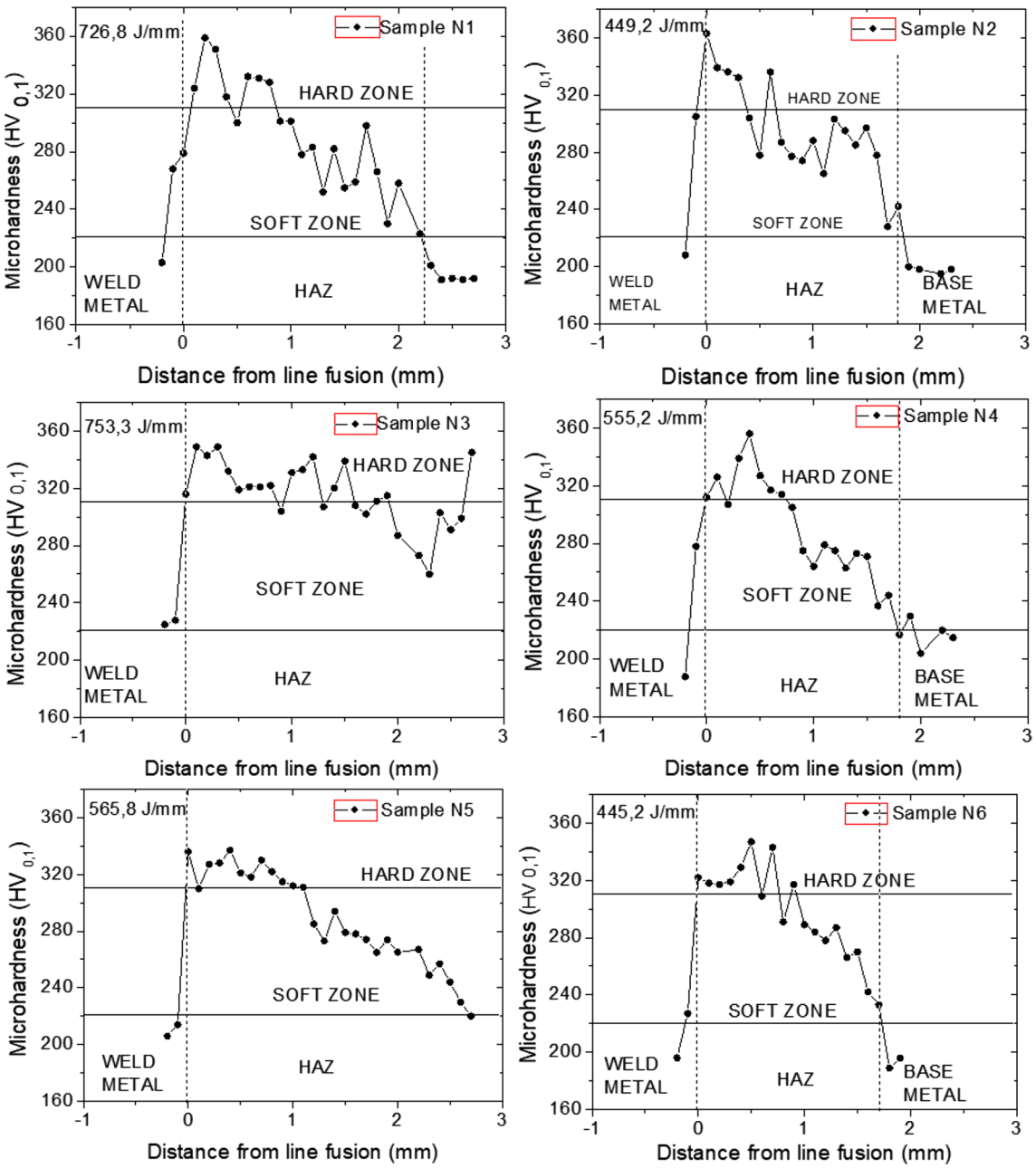

Fig. 5 Cross-sectional microhardness profiles of the deposited passes with different levels of welding energy using the Inconel 625 wire

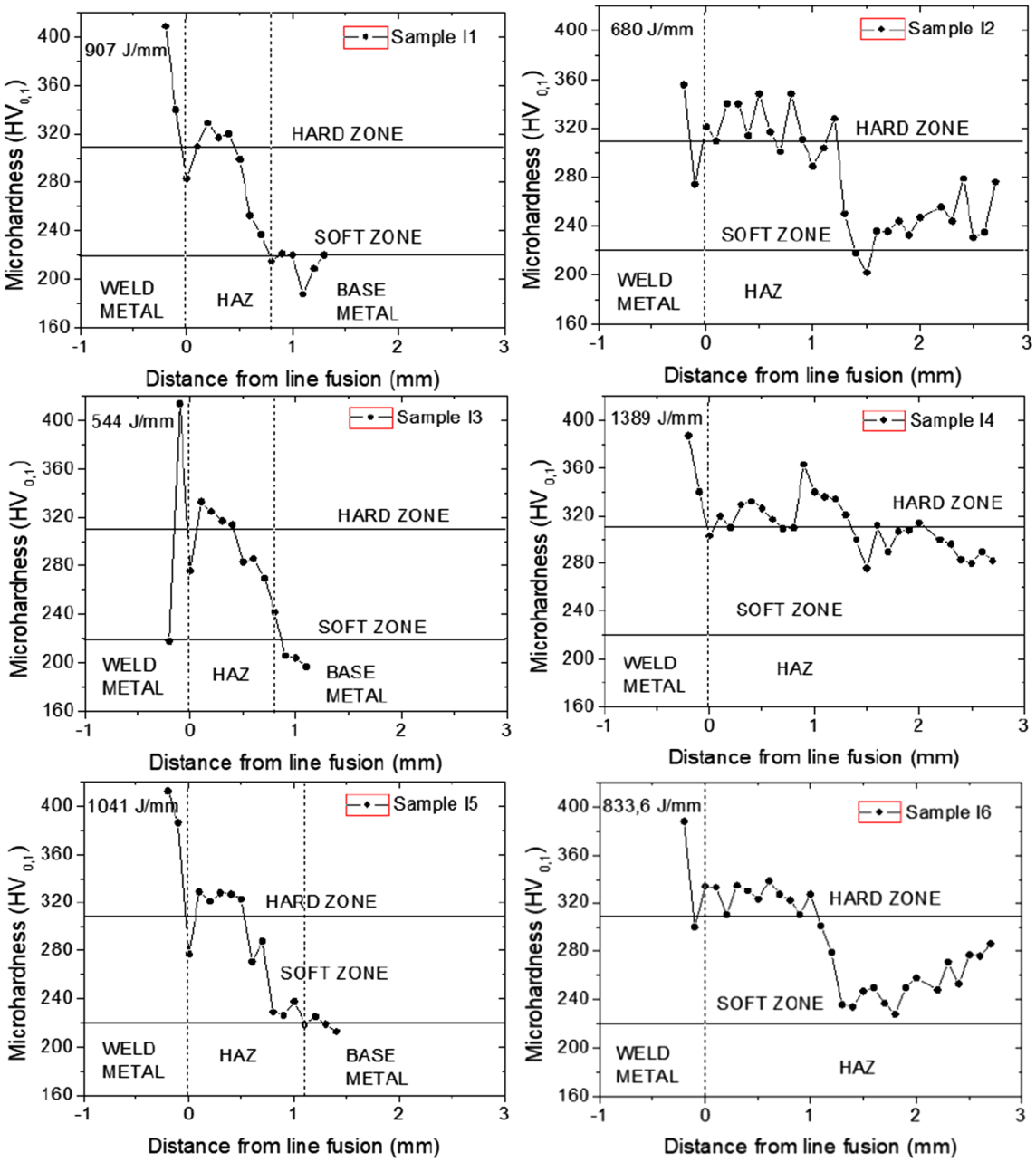

Fig. 6 Cross-sectional microhardness profiles of the deposited passes with different levels of welding energy using the ER 309L-Si wire

309L-Si and 80S-G wires, respectively. In HAZ, there is a high-hardness region adjacent to the weld bead with values around 350 HV known as HZ. Another region with the decrease in hardness values can be observed which is known as SZ, which must overlap the high-hardness regions in the two-layer welding to cause tempering and, consequently, HZ hardness reduction.

The data given in Table 4 present the extension of the hard (re-austenitized) and soft zones (tempered), along with the mean values for reinforcement and penetration of the single weld beads.

The Higuchi graphs (Fig. 8) were based on the presented values in Table 4. In these graphs, the attended or not attended of the established criteria by Higuchi [19] is confirmed in Eqs. 1 and 2. In the first condition analysis (Eq. 1), the positive values of $\Delta 1$ are considered satisfactory, since they indicate that SZD2 is greater than HZD1. This first condition revealed that the heat input in the second layer needs to be higher than the first, because high welding heat input in the first layer difficulties the temper in the first-layer HZ by applying a second layer with less energy. In addition, although the Higuchi test did not take into account

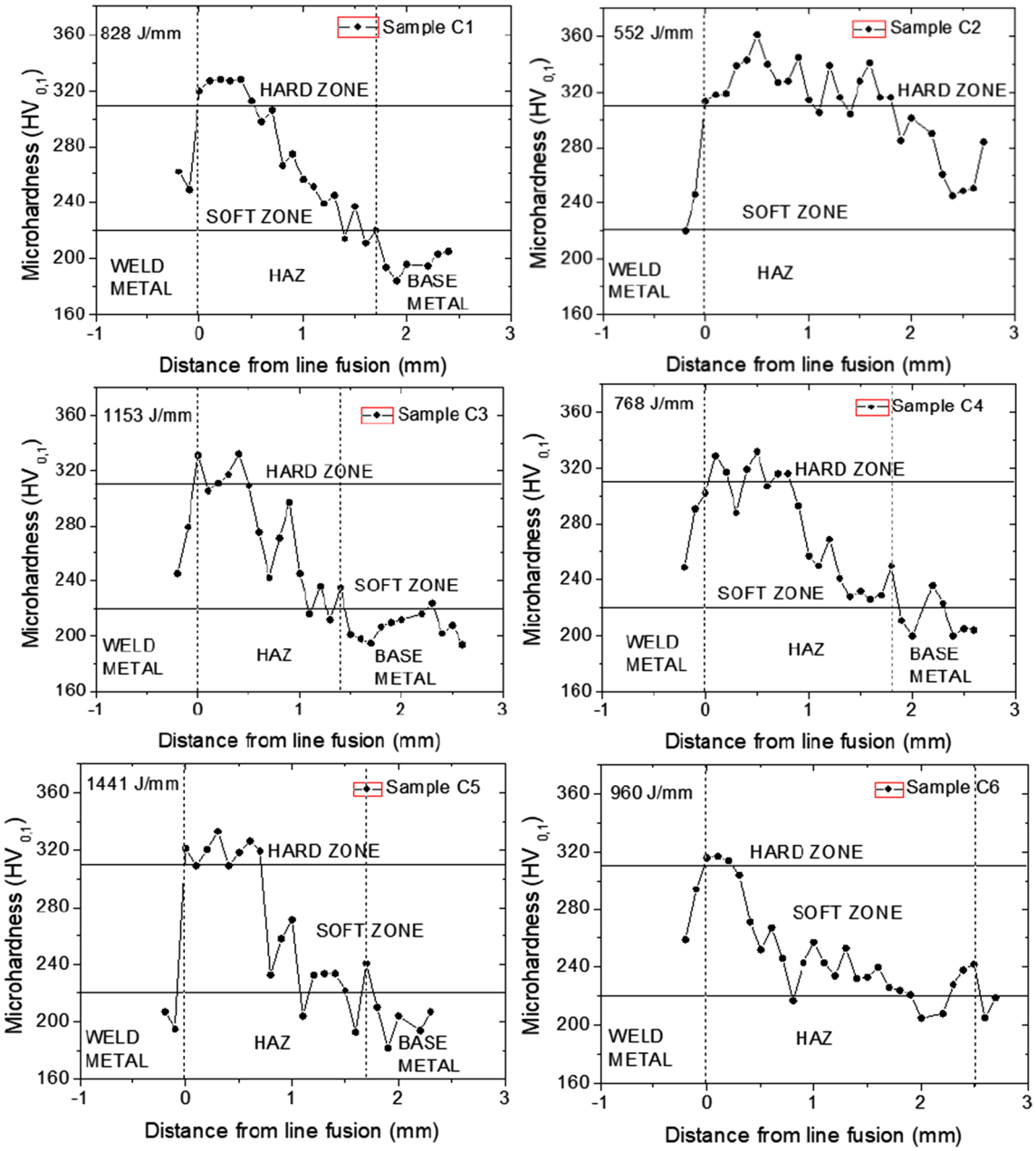

Fig. 7 Cross-sectional microhardness profiles of the deposited passes with different levels of welding energy using the ER 80S-G wire

the microstructural changes, the use of high energy in the first layer causes a high grain growth, making it difficult to refine the CGHAZ in the second-layer deposition.

The second condition (Eq. 2) is considered satisfactory, when the Δ2 values are greater than or equal to zero and unsatisfactory for negative values. Positive values indicate that the second-layer HZ would be contained in the weld metal of the first layer and it is not a critical region. On the other hand, negative values indicate a re-austenization on the first-layer CGHAZ, creating a high-hardness region. Fulfilling both conditions ensures that the energy ratio can be selected for double-layer welding without compromising the hardness and toughness of the material [24, 25].

Figure 9 shows the decision diagrams used in the selection of the best welding energies for first- and second-layer deposition, simulating the possibilities of double-layer deposition considered for conditions C1 and N5 on the first layer and considering the different filler metals and welding conditions of Table 2, for the second layer. The analysis of these diagrams indicates that the acceptance criterion of Eqs. 1 and 2 was met for the following energy ratios (first layer/second layer): C1/C6, Fig. 9a, N5/C6 and N5/I2 Fig. 9b.

Table 4 Extension values (mm) of various weld regions for ASTM A182 F22 steel Higuchi test

Condition	Wire	Welding heat input (J/mm)	*R*	*P*	HZ (mm)	SZ (mm)	HZD	SZD
N1	Inconel 625	726.8	2.6	2.2	0.9	1.3	5.7	4.4
N2		449.2	2.8	1.5	0.4	1.5	4.6	3.4
N3		753.3	3.2	1.7	2.7	1.0	7.6	5.4
N4		555.2	2.7	2.1	0.8	1.0	5.6	3.9
N5		565.8	2.7	1.2	1.2	1.5	5.1	3.9
N6		445.2	2.2	1.5	1.0	0.8	4.7	3.3
I1	309L-Si	907.2	2.9	3.8	0.4	0.6	7.0	4.8
I2		680.1	2.5	3.3	1.3	5.7	7.2	10.3
I3		544.5	2.4	2.6	0.4	0.4	5.4	3.4
I4		1388.8	2.6	4.6	2.1	2.8	9.3	9.4
I5		1041.1	2.6	4.3	0.5	0.6	7.4	5.4
I6		833.6	2.6	3.8	1.1	5.3	7.6	10.3
C1	80S-G	828.8	2.3	2.2	1.2	0.9	5.7	4.3
C2		552.0	2.2	1.7	0.9	0.6	4.7	3.2
C3		1153.1	2.7	3.8	0.6	0.6	7.1	5.0
C4		768.0	2.4	3.0	0.9	1.2	6.3	5.1
C5		1441.4	3.3	3.7	0.9	0.7	7.8	5.3
C6		960.0	2.9	3.6	0.4	2.3	6.9	6.3

R reinforcement, *P* penetration, *HZ* hard zone depth, *SZ* soft zone depth, *HZD* first-layer hard zone depth, *SZD* second-layer soft zone depth

These graphs show the HAZ behavior as a function of the thermal cycle on the second layer in different combinations used for Higuchi test.

The conditions below the reference line should not be employed because of the risk in a re-austenization by the extension of the first-layer hard zone and, depending on the cooling rate in this region, in a re-temper.

From Fig. 9a, it is observed that through all acceptable welding parameter possibilities for the second layer, considering the C1 condition for the first layer, only the C6 condition was satisfactory with positive deviation from the reference line. In Fig. 7b, this parameters' combination is represented by the condition N5 in the first layer and the condition I2 in the second layer. Although the combination N5/C6 also satisfies the adopted criteria, it is not interesting from the metallurgical point of view since it would produce another interface between dissimilar materials.

The analysis of the decision diagrams in Fig. 9 shows that the first layer is deposited with low welding energy. This implies that the tempering condition (SZD2 > HZD1) of the CGHAZ of the first layer would not be satisfied if the subsequent layer has a low-energy condition. In this case, the thermal cycle responsible for tempering the first-layer HAZ would not extend the hard zone completely.

On the other hand, the conditions with higher thermal input for the second layer attend better the previous criteria. But the second tempering criteria (R1 + P1 > HZD2) begin to suffer a significant change, that for low energy in the second layer did not present problems, began to present negative values due to the low values in first-layer reinforcement and penetration when compared to the second-layer hard zone extensions. With the high energy in the first-layer deposition, the first tempering criteria (SZD2 > HZD1) would not be satisfied for all the energy bands in the second layer since the increase in the thermal input is associated with the great depths of hard zone.

3.2 Microstructural characterization of HAZ

During welding, the thermal cycles produce distinct microstructures, leading to variation in mechanical properties as observed in microhardness profiles, as shown in Figs. 5, 6 and 7. The microstructure of the HAZ is not uniform with the formation of different regions, as shown in Fig. 10. The peaks of temperature are larger near the melting line and progressively decrease to the base metal. The microstructure developed inside of each zone is a direct result of the thermal cycling in each location.

Figure 10a shows the microstructure of the HAZ near the interface (hard zone). This region is identified as the coarse-grained HAZ (CGHAZ). The microstructure present is formed by bainite which structure is responsible for the high-hardness values. Different authors also mention the presence of carbides such as $M_{23}C_6$ and M_2C [4, 6, 26, 31]. However, it was believed that due to the high temperature reached during the welding operation, there is dissolution or

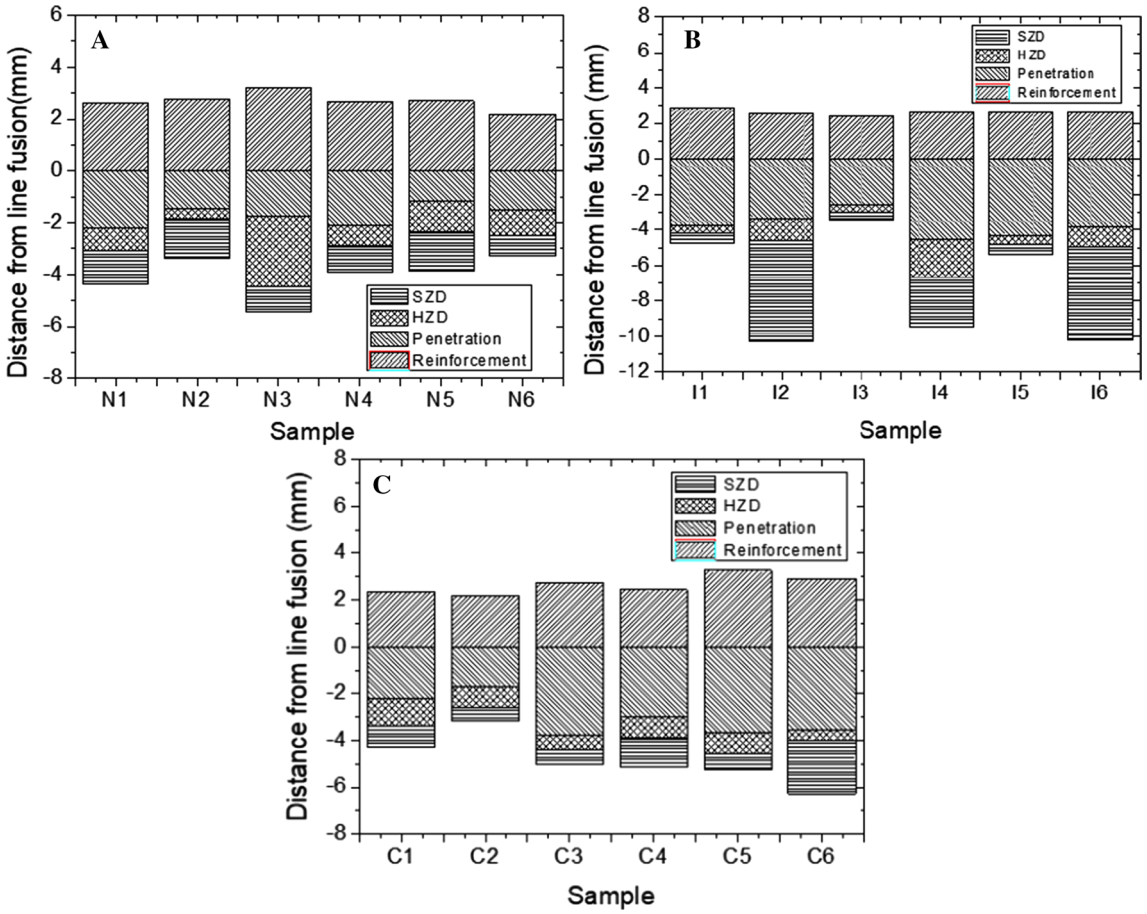

Fig. 8 Higuchi graph for welded samples with different filler materials, **a** Inconel 625, **b** ER 309L-Si and **c** 80S-G

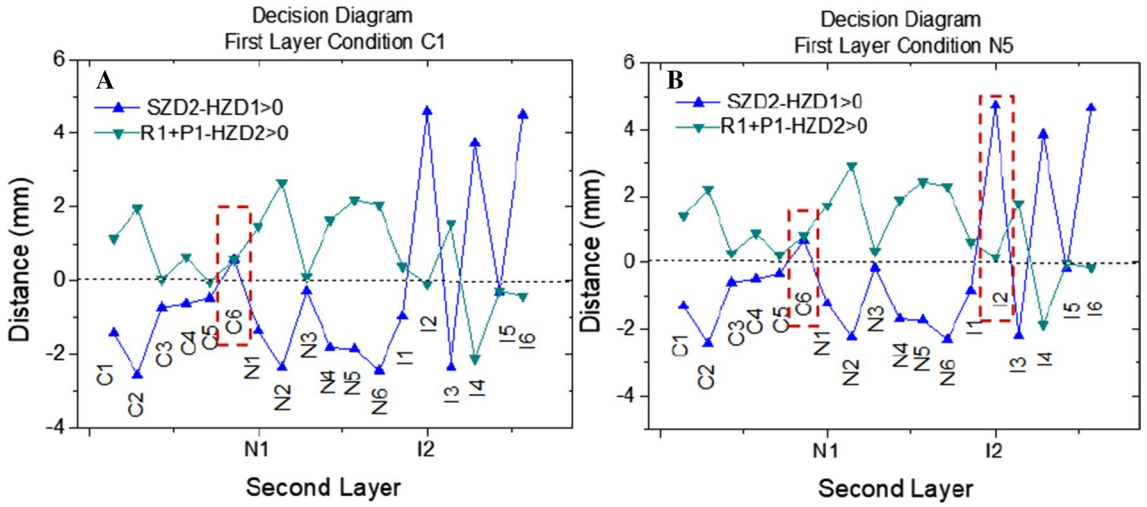

Fig. 9 Decision diagram: **a** for condition C1 in the first layer and **b** for the condition N5 in the first layer

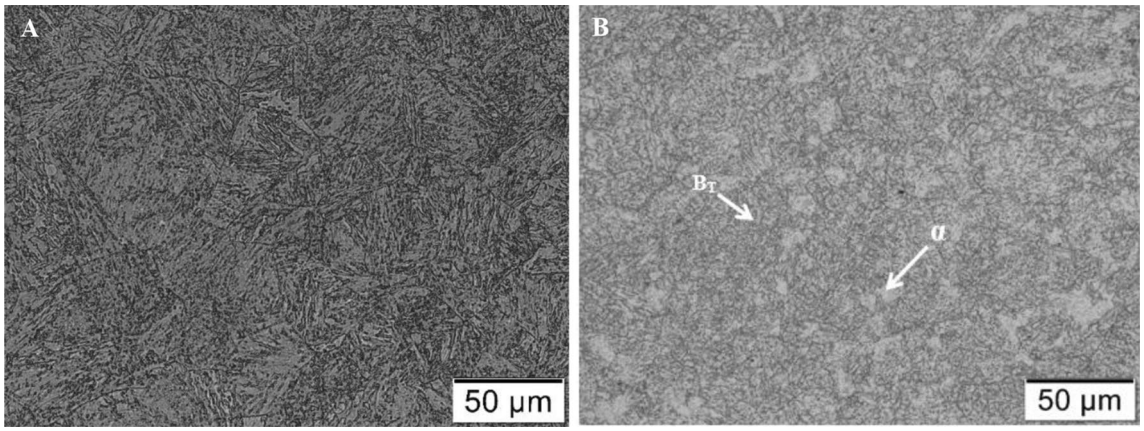

Fig. 10 Microstructure of the different regions in HAZ, **a** CGHAZ and **b** FGHAZ

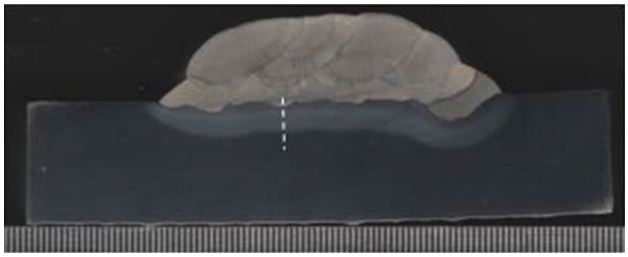

Fig. 11 Double-layer welding using N5/I2 relation. Nital 10% etch

a reduction of the carbides, which caused the grain size to increase in this region.

In Fig. 10b, the microstructure of the fine-grained HAZ (FGHAZ) can be observed. It is possible to observe two phases and smaller grains and verify that a non-uniform microstructure was created by ferrite (α-Fe) and transformed bainite (TB) phases. There is a reduction in the hardness values in this region by the presence of ferrite.

3.3 Two-layer deposition

In this step, for the double-layer welding, two energy relations were selected for the validation of the Higuchi method. The energy ratios of N5/I2 and C1/C6 were approved, as shown in the decision diagram in Fig. 9. Figure 11 presents a cross-sectional macrography extracted from a double-layer weld sample using N5/I2 relation. The cross sections of the double-layer welds revealed a defect-free interface between passes.

In Fig. 12, the microhardness profiles of the first-layer HAZ of double-layer welds can be seen, for relations N5/I2 and C1/C6, and can be compared to the values found in the HAZ of single-pass weld beads C1 and N5 from Figs. 7

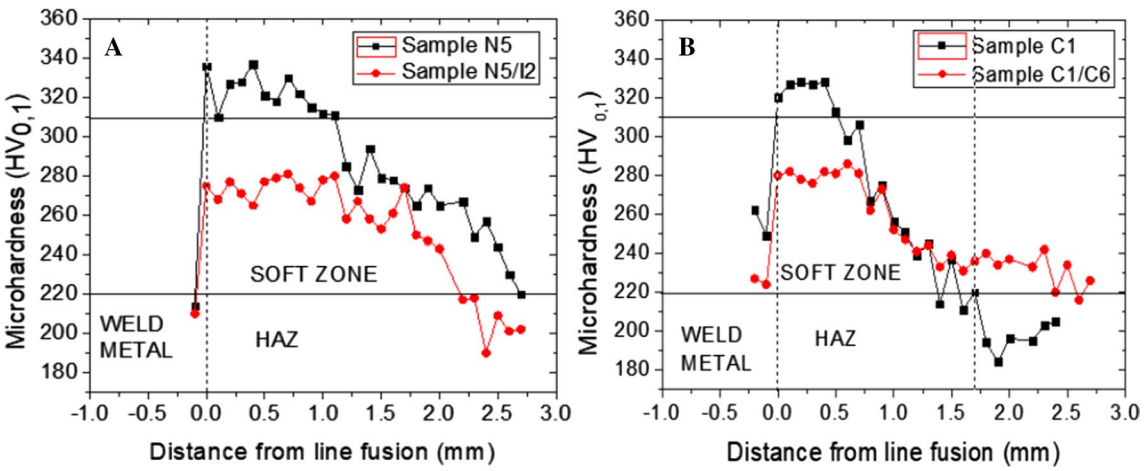

Fig. 12 Microhardness profiles of two-layer deposition samples and single-pass samples, without PWHT. **a** Samples N5 and N5/I2, and **b** samples C1 and C1/C6

and 5, respectively. It is worth mentioning that on the ends of the cladding (start and end), the double-layer technique is not effective since in these regions the correct overlapping of the weld beads is not guaranteed.

The technique effectiveness is assured mainly from the third weld bead of the second layer, since the overlapping stabilizes on this region chosen for the HAZ microhardness test as shown in Fig. 11.

The microhardness profiles collected from the HAZ of double-layer welds sample, as shown in Fig. 12, revealed the Higuchi test effectiveness over the tempering (hardness reduction) promoted by the thermal cycle of the second layer over the first-layer HAZ on F22 steel. The elimination of the hardness peaks from the hard zone (above 310 HV) can be seen, when compared to the single weld bead condition. Such behavior is due to the tempering effect from side and subsequent passes, as long as there is no re-austenitization on the first layer above approximately 1000 °C, because, during the posterior cooling, hard bainite without tempering would appear. This re-temper impairs the objectives of the double-layer technique.

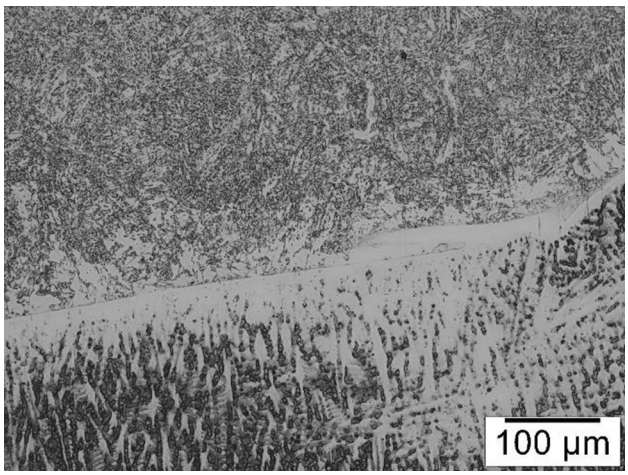

Fig. 13 First-layer HAZ microstructure for an approved energy relation from Higuchi test, N5/I2 sample

The microstructure found in the first-layer CGHAZ for approved energy relations on Higuchi test is composed mainly by ferrite and tempered bainite, as shown in Fig. 13, therefore from the tempering effect promoted by the thermal cycles from the second-layer deposition.

Although the microhardness profiles shown in Fig. 12 demonstrate the efficiency of the double-layer technique (Higuchi test) to reduce the hardness in the first-layer HAZ in the base metal by the hard zone elimination, the double-layer technique was not able to reduce the hardness below 250 HV established by NACE MR0175 standard. This condition was reached with the PWHT, as shown in Fig. 14.

It is believed that the longer time (2 h) on a high temperature (675 °C) during the PWHT was more effective in the decomposition of bainite in ferrite, when compared to the overlapping of welding thermal cycles, as shown in Fig. 15, allowing a more significant hardness reduction.

Figure 16 presents the different microstructures of the region next to the interface between the weld metal and HAZ. In the Inconel 625 weld metal interface without PWHT (Fig. 16a) and with PWHT (Fig. 16b), it is possible to observe the decarburization of the F22 HAZ. The overlapping thermal cycles on the double-layer deposition as well as the preheating and interpasses temperatures, contributed for the carbon migration from the base metal toward the weld metal, cause decarburization phenomenon (Fig. 16a), although in a less effective way, since a darker region was not noticed on the dissimilar interface. The darker region observed on the dissimilar interface (Fig. 16b) with PWHT is a result of the carbon diffusion from the base metal toward the weld metal; this phenomenon creates a region with lower

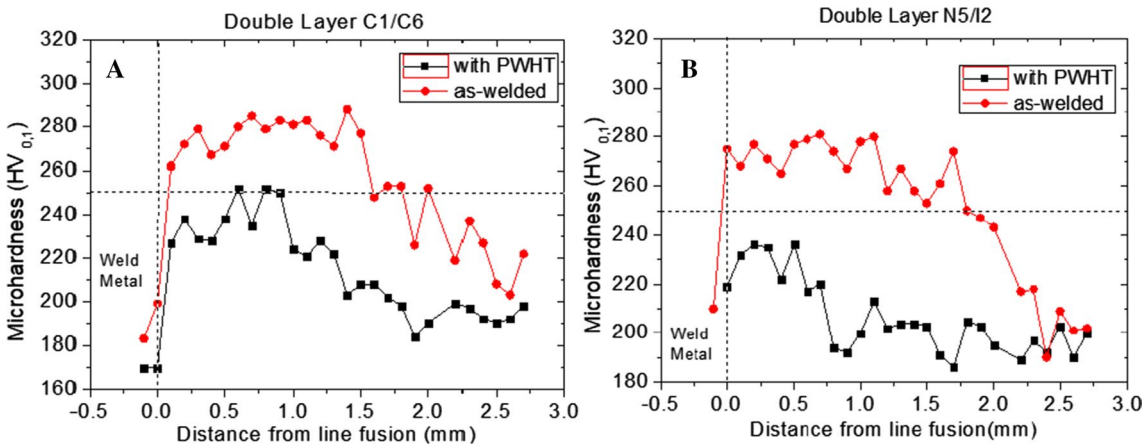

Fig. 14 Microhardness profiles of the two-layer deposition samples with and without PWHT: **a** C1/C6 ratio and **b** N5/I2 ratio

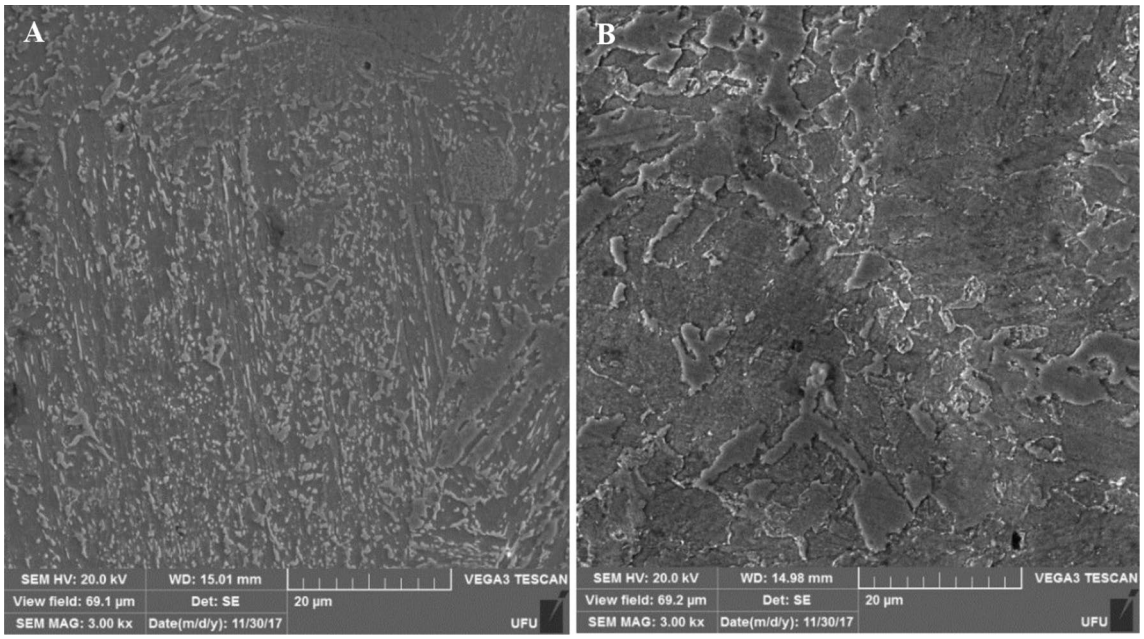

Fig. 15 SEM of the CGHAZ with the condition N5/I2: **a** without PWHT and **b** with PWHT

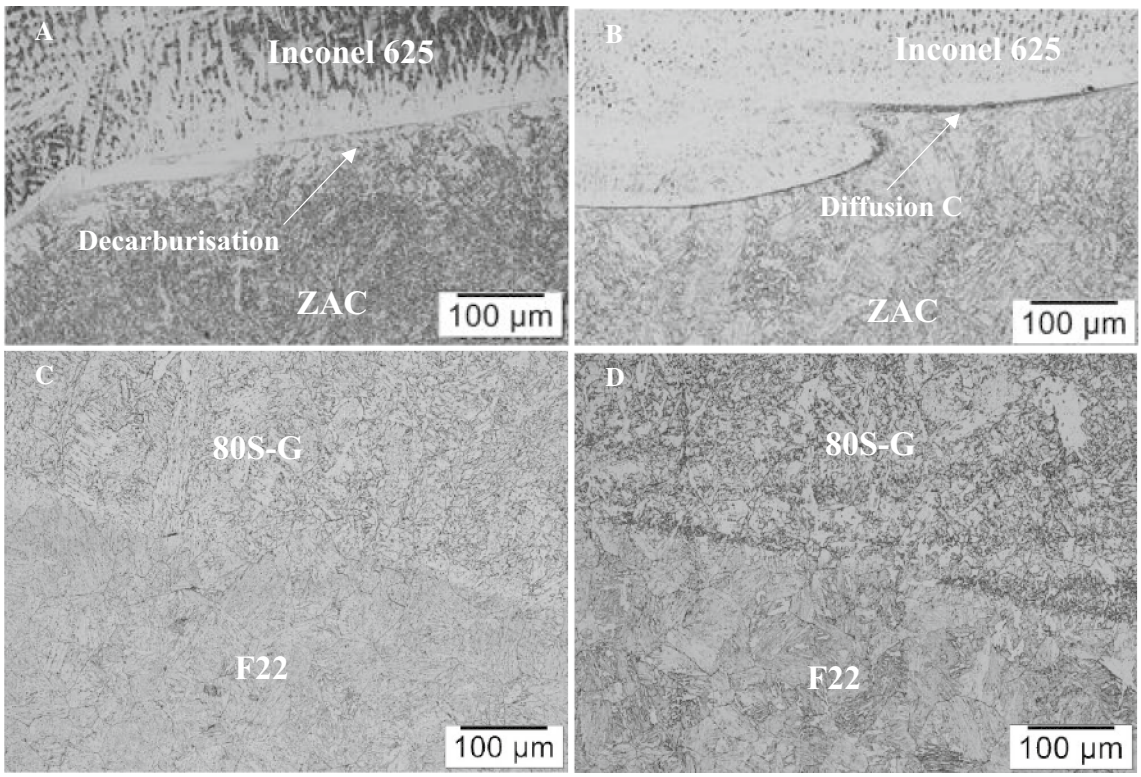

Fig. 16 Optical micrograph of the interface HAZ/double layer: **a** Inconel without PWHT, **b** Inconel with PWHT, **c** 80S-G without PWHT and **d** 80S-G with PWHT

carbon content (decarburization) adjacent to the dissimilar interface on the base metal side [10–12, 27–30].

The formation of this microstructure on the interface of the dissimilar weld is widely disseminated in the literature [10, 11, 27–31]. This region is susceptible to cracks nucleation and propagation due to the rise in microhardness.

The micrographs of the interface region of the weld F22/80S-G with and without heat treatment are shown in Fig. 16c, d, respectively. The images show that there was no decarburization on the HAZ, probably due to the similar chemical composition of the base and filler metal. The mixture of the material on the fusion line does not produce distinct phases and will not cause any significant change in mechanical properties.

4 Conclusion

Based on the experimental results, it was possible to reach the following conclusions:

The geometry of the weld bead directly affects the double-layer technique, which justifies the reduced number of welding energy ratios approved for different wires.

The two-layer deposition technique efficiency was generally approved for reduced heat input conditions in the first layer, and the hardness of the HAZ without PWHT had a reduction below 300 HV.

It can be observed that the higher the energy for the first-layer deposition, the greater the hard zone or the CGHAZ, which hinders the complete tempering of this region by the second-layer thermal cycle.

The results showed that the double-layer technique performed in this work could not reduce the hardness at 250 HV required by NACE 0175. That was possible only with PWHT, which caused a greater bainite in ferrite decomposition.

The HAZ generated by the Higuchi technique presented a grain refinement due to the overlapping of the welding thermal cycles, less carbon diffusion and the decarburization effect on the dissimilar interface (Inconel 625/F22) when compared with the condition submitted to PWHT. This phenomenon was not noticed on the interface formed with the low-alloy filler metal (80S-G).

Acknowledgements The authors express their gratitude to institutions that supported this work as FAPEMIG, UFU and UFPA.

References

1. Tsay LW, Lin WL, Cheng SW, Leu GS (1997) Hydrogen sulphide stress corrosion cracking of 2.25Cr-Mo steel weldments. Corros Sci G B 39(7):1165–1176. https://doi.org/10.1016/s0010-938x(97)00015-2
2. Parameswaran P, Paul VT, Vijayalakshmi M, Raghunathan VS (2004) Microstructural evolution in a single pass autogenously welded 2.25Cr–1Mo steel. Trans Indian Inst Met J Nucl Mater Indian 58(3):253–264
3. Thomson RC, Miller MK (1998) Carbide precipitation in martensite during the early stages of tempering Cr- and Mo-containing low alloy steels. Acta Mater 46(6):2203–2213. https://doi.org/10.1016/s1359-6454(97)00420-5
4. Peddle BE, Pickles CA (2000) Carbide and hardness development in the heat affected zone of tempered and postweld heat-treated 2.25Cr–1Mo steel weldments. J Mater Eng Perform USA 9(5):477–488. https://doi.org/10.1361/105994900770345593
5. Miranda RM, Fortes MA (1989) Austenite grain growth, microstructure and hardness in the heat-affected zone of a 2.25 Cr- 1Mo steel. Mater Sci Eng. https://doi.org/10.1016/0921-5093(89)90399-7
6. Parvathavarthini N, Saroja S, Dayal RK, Khatak HS (2001) Studies on hydrogen permeability of 2.25Cr–1Mo ferritic steel: correlation with microstructure. J Nucl Mater G B. https://doi.org/10.1016/s0022-3115(00)00706-6
7. Irving B (1995) The challenge of welding heat treatable alloy steels. Weld J 74(2):43–48
8. Graville BA (1976) Cold cracking in welds in HSLA steels. Welding of HSLA (microalloyed) structural steels. In: Proceedings of international conference. American Society for Metals
9. ASTM A182 (2005) Standard specification for forged or rolled alloy and stainless steel pipe flanges, forged fittings, and valves and parts for high-temperature service. West Conshohocken. https://doi.org/10.1520/a0182_a0182m-14a
10. Dupont JN, Kusko CS (2007) Technical note: martensite formation in austenitic/ferritic dissimilar alloy welds. Weld J 86:983–989
11. Olden V, Kvaale PE, Simense PA, Aaldstedt S, Solberg JK (2003) The effect of PWHT on the materials properties and microstructure in Inconel 625 and Inconel 725 buttered joints. OMAE 2003. Paper No. 37196. OMAE, Cancun, Mexico. https://doi.org/10.1115/omae2003-37196
12. Dodge MF, Dong HB, Milititski M, Barnett RP, Gittos MF (2013) Environment-induced cracking in weld joints in subsea oil and gas systems –part II. In: 32nd international conference on ocean, offshore and arctic engineering, 2013, Nantes, France. https://doi.org/10.1115/omae2013-10339
13. Nino CE, Correa JA, Buschinelli AJA (1992) Técnicas de reparo por soldagem em aços 5Cr–0,5Mo. Sold Mater 4(2):28–33 **in Portuguese**
14. Teixeira JCG, Pope AM (1992) Técnica de Deposição em Dupla-Camada para Reparo e Modificações e Tratamento Térmico Pós-Soldagem de Aço 1Cr–0,5Mo. Soldagem e Materiais 4(2):23–27
15. Niño CE, Buschinelli AJA (1995) Análise de alternativas de reparo por soldagem de aços Cr–Mo. In: XXI Encontro Nacional de Tecnologia de Soldagem, Caxias do Sul, Brazil, 1995, in Portuguese. https://doi.org/10.26678/abcm.cobef2017.cof2017-0066
16. Bueno ER (1999) Desenvolvimento do Procedimento de Soldagem do AISI 4140 sem Tratamento Térmico Posterior. Dissertation. University of Federal de Santa Catarina
17. Henke SL, Niño CE, Buschinelli AJA (2000) Soldagem dissimilar do aço CA-6NM sem tratamento térmico posterior. Soldagem & Materiais, São Paulo, vol 6, no 1, p 1–9
18. Lant T, Robinson DL, Spafford B, Storesund J (2001) Review of weld repair procedures for low alloy steels designed to minimize the risk of future cracking. Int J Press Vessels Pip 78:813–818. https://doi.org/10.1016/s0308-0161(01)00094-1
19. Higuchi M, Sakamoto H, Tanioka S (1980) A study on weld repair through half bead method. IHI Eng Rev 13:14–19
20. Dupont JN, Banovic SW, Marder AR (2003) Microstructural evolution and weldability of dissimilar welds between a

super austenitic stainless steel and nickel based alloys. Weld J 82(6):125–156. https://doi.org/10.1179/136217102225006804
21. DODGE MF (2014) The effect of heat treatment on the embrittlement of dissimilar welded joints. 228 f. Thesis Doctor—University of Leicester
22. Aloraier A, Ibrahim R, Thomsom P (2006) FCAW process to avoid the use of post weld heat treatment. Int J Press Vessels Pip 2006(83):394–398. https://doi.org/10.1016/j.ijpvp.2006.02.028
23. Aloraier A, Ibrahim RN, Ghojel J (2004) Eliminating post-weld heat treatment in repair welding by temper bead technique: role bead sequence in metallurgical changes. J Mater Process Technol 153–154:392–400. https://doi.org/10.1016/j.jmatprotec.2004.04.383
24. Silva CC, Albuquerque VHC, Moura CRO, Aguiar WM, Farias JP (2009) Evaluation of AISI 4140 steel repair without post-weld heat treatment. J Mater Eng Perfor UK 18(3):324–331. https://doi.org/10.1007/s11665-008-9294-5
25. Cavalcante NE, Andrade TC, Pinheiro PHM, Miranda HC, Motta MF, Aguiar WM (2016) Estudo de Procedimentos de Soldagem MIG/MAG para Aplicação de Revestimentos de Liga de Níquel Inconel 625 em Aço Estrutural ASTM A387 Gr.11. Soldagem Inspeção São Paulo 21(1):70–82. https://doi.org/10.1590/0104-9224/si2101.07
26. Hodgson DK, Dai T, Lippold JC (2015) Transformation and tempering behavior of the heat-affected zone of 2.25Cr–1Mo steel. Weld J Miami 94:250–256
27. Garcia DN (2018) Mechanical and metallurgical behavior of steel welded joint ASTM A182 F22 Applied in the Offshore Industry. 2018. 209 f. Thesis Doctor—, Federal University of Uberlandia
28. Alexandrov BT, Lippold JC, Sowards JW, Hope AT, Saltzmann DR (2012) Fusion boundary microstructure evolution associated with embrittlement of Ni–base alloy overlays applied to carbon steel. Weld World Paris 57(1):39–53. https://doi.org/10.1007/s40194-012-0007-1
29. Fenske JA (2010) Microstructure and hydrogen induced failure mechanisms in iron nickel weldments. 163 f. Thesis Doctor—University of Illinois, Urbana
30. Da Mota CAM, Nascimento AS, Garcia DN, Silva DAS, Teixeira FR, Ferraresi VA (2017) Revestimento de Níquel Depositado pela Soldagem MIG e MIG com Arame Frio. Revista Soldagem e Inspeção 21:483–496. https://doi.org/10.1590/0104-9224/si2104.08
31. Teixeira FR, Da Mota CAM, De Almeida HAL, Scotti A (2019) Operational behavior of the switchback GMAW process using a mechanized rig for arc movement. J Mater Process Technol 269:135–149. https://doi.org/10.1016/j.jmatprotec.2019.02.014